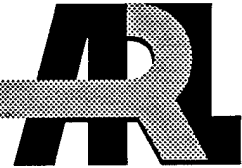


ARMY RESEARCH LABORATORY



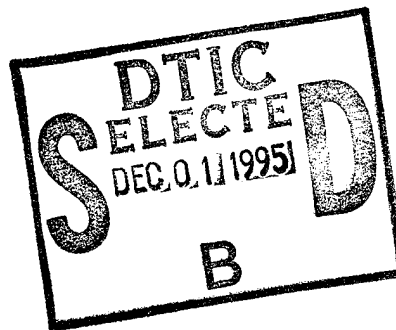
Navier-Stokes Computations for a Reacting, M864 Base Bleed Projectile

Charles J. Nietubicz
U.S. ARMY RESEARCH LABORATORY

Howard J. Gibeling
SCIENTIFIC RESEARCH ASSOCIATES, INC.

ARL-TR-875

October 1995



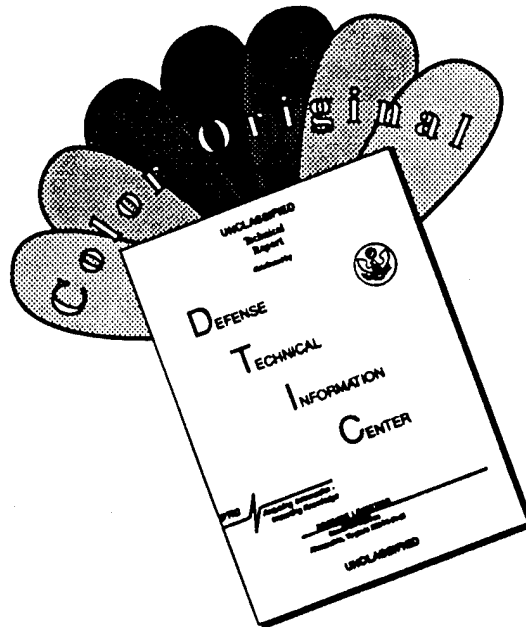
19951130 070

DTIC QUALITY INSPECTED 8

APPROVED FOR PUBLIC RELEASE; DISTRIBUTION IS UNLIMITED.

DTIC QUALITY INSPECTED 8

DISCLAIMER NOTICE



THIS DOCUMENT IS BEST QUALITY AVAILABLE. THE COPY FURNISHED TO DTIC CONTAINED A SIGNIFICANT NUMBER OF COLOR PAGES WHICH DO NOT REPRODUCE LEGIBLY ON BLACK AND WHITE MICROFICHE.

REPORT DOCUMENTATION PAGE			Form Approved OMB No. 0704-0188	
Public reporting burden for this collection of information is estimated to average 1 hour per response, including the time for reviewing instructions, searching existing data sources, gathering and maintaining the data needed, and completing and reviewing the collection of information. Send comments regarding this burden estimate or any other aspect of this collection of information, including suggestions for reducing this burden, to Washington Headquarters Services, Directorate for Information Operations and Reports, 1215 Jefferson Davis Highway, Suite 1204, Arlington, VA 22202-4302, and to the Office of Management and Budget, Paperwork Reduction Project (0704-0188), Washington, DC 20503.				
1. AGENCY USE ONLY (Leave blank)		2. REPORT DATE October 1995	3. REPORT TYPE AND DATES COVERED Final, Jan 92 - Jan 93	
4. TITLE AND SUBTITLE Navier-Stokes Computations for a Reacting, M864 Base Bleed Projectile			5. FUNDING NUMBERS PR: 1L161102AH43 WO: 61102A-00-001-AJ	
6. AUTHOR(S) Charles J. Nietubicz and Howard J. Gibeling*				
7. PERFORMING ORGANIZATION NAME(S) AND ADDRESS(ES) U.S. Army Research Laboratory ATTN: AMSRL-WT-PB Aberdeen Proving Ground, MD 21005-5066			8. PERFORMING ORGANIZATION REPORT NUMBER ARL-TR-875	
9. SPONSORING / MONITORING AGENCY NAME(S) AND ADDRESS(ES)			10. SPONSORING / MONITORING AGENCY REPORT NUMBER	
11. SUPPLEMENTARY NOTES * Howard J. Gibeling is currently employed by Carrier Corporation, P.O. Box 4808, Syracuse, NY 13221.				
12a. DISTRIBUTION / AVAILABILITY STATEMENT Approved for public release; distribution is unlimited.			12b. DISTRIBUTION CODE	
13. ABSTRACT (Maximum 200 words) The M864 projectile is an extended range design which includes both a dome base cavity and a base burn capability. The extended range is accomplished through the injection of hot, fuel-rich gas which burns in the initially low-pressure base region. The present analysis utilizes a Navier-Stokes computational technique which includes finite rate chemistry to model the reacting base flow region for the M864. Calculations have been performed for the full projectile configuration, including the base region for a Mach number range of $0.8 \leq M \leq 3.0$. The reacting gas was modeled as a mixture of H_2 and CO. Calculations show a significant increase in base pressure with the injection of both H_2 and CO due to the more distributed nature of the base combustion and the higher wake region temperatures. Computations were obtained at Mach = 3.0 for conditions of no bleed, nonreacting hot gas injection, and H_2 and CO injection. Results are presented in the form of temperature contours and velocity vectors in the near-wake region for this case. Comparisons of the computed drag coefficient, C_{D_0} , are made with trajectory model predictions based on actual range firings of the M864.				
14. SUBJECT TERMS projectiles, drag, base burn, Navier-Stokes equations, M864, extended range, CFD			15. NUMBER OF PAGES 30	
			16. PRICE CODE	
17. SECURITY CLASSIFICATION OF REPORT UNCLASSIFIED	18. SECURITY CLASSIFICATION OF THIS PAGE UNCLASSIFIED	19. SECURITY CLASSIFICATION OF ABSTRACT UNCLASSIFIED	20. LIMITATION OF ABSTRACT UL	

INTENTIONALLY LEFT BLANK.

TABLE OF CONTENTS

	<u>Page</u>
LIST OF FIGURES	v
1. INTRODUCTION	1
2. GOVERNING EQUATIONS AND SOLUTION TECHNIQUE	3
2.1 Governing Equations	3
2.2 Turbulence Model	6
2.3 Chemistry Model	7
2.4 Boundary Conditions	8
2.5 Solution Technique	10
2.6 Computational Grid	10
2.7 Results	12
3. SUMMARY	20
4. REFERENCES	21
DISTRIBUTION LIST	25

Accession For	
NTIS GRA&I	<input checked="" type="checkbox"/>
DTIC TAB	<input type="checkbox"/>
Unannounced	<input type="checkbox"/>
Justification	
By	
Distribution/	
Availability Codes	
Dist	Avail and/or Special
A-1	

INTENTIONALLY LEFT BLANK.

LIST OF FIGURES

<u>Figure</u>	<u>Page</u>
1. Schematic of M864 base bleed projectile	2
2. M864 base burn motor	3
3. M864 computational model	11
4. Computational grid near projectile surface	11
5. M864 base region grid	13
6. Temperature contours, hot air injection, $M_\infty = 2.0$, $T = 1,533$ K	13
7. Temperature contours, H_2 -CO injection, $M_\infty = 2.0$, $T_j = 1,533$ K	14
8. Temperature contours, H_2 -CO injection, $M = 3.0$	14
9. Comparison of temperature contours, $M = 1.5$ (bottom) and $M = 3.0$ (top)	16
10. Species mass fraction contours for CO, $M = 3.0$	16
11. Comparison of species mass fraction for CO, $M = 1.5$ (bottom) and $M = 3.0$ (top) ..	17
12. Mach contours, $M_\infty = 3.0$	17
13. Comparison of Mach contours, $M_\infty = 1.5$ (bottom) and $M_\infty = 3.0$ (top)	18
14. Base pressure vs. radial position	18

INTENTIONALLY LEFT BLANK.

1. INTRODUCTION

The ability to compute the base region flow field for projectile configurations using Navier-Stokes computational techniques has been of active interest within the Aerodynamics Branch of the Propulsion and Flight Division, U.S. Army Research Laboratory, for the past decade. These techniques are most important for determining aerodynamic coefficient data which depend on the coupled viscous and inviscid interacting flow fields. Particular emphasis has been placed on predictions of the total aerodynamic drag. The total drag as described in this report consists of the pressure drag (excluding the base), viscous drag, and base drag components. At transonic and low supersonic speeds, the base drag component is the major contributor to the total aerodynamic drag.

Since aerodynamic drag has the greatest impact on the eventual range of an artillery shell, any reduction in drag can have a large payoff in increased range. An effective means for reducing drag is through the addition of mass in the low-speed, recirculating, low-pressure region directly behind the projectile base. This technique is known as "base bleed" and has been the subject of experimental (Baker, Davis, and Matthews 1951; Murthy et al. 1976; Murthy and Osborn 1976; Strahle, Hubbart, and Walterick 1982) and computational studies (Sahu, Nietubicz, and Steger 1985; Sahu 1986). When the gas is combustible, an additional drag reduction is obtained due to the wake burning which occurs. The latter technique is termed "base burn" and was initially described by Baker, Davis, and Matthews (1951).

The application of advanced numerical techniques to base bleed projectile configurations was first begun by Sahu (1986). In the initial work, the projectile base was considered to be flat, and cold mass injection was modeled. As interest extended to the M864 projectile, the effect of a domed base configuration as well as the injection of hot mass injection was studied by Nietubicz and Sahu (1988). The results of this work, coupled with experimental ground-based tests, led to the development of an engineering model by Danberg (1990) for the prediction of flight performance of the M864 as well as other base bleed projectiles (Danberg 1991). The next effort was to provide a combustion capability which was developed by Gibeling and Buggeln (1991), where they extended the Scientific Research Associates, Inc. (SRA) MINT and CMINT codes to a flat base projectile and investigated various combustion models.

The M864 is a 155-mm, extended range, cargo-carrying projectile shown in Figure 1. It has a boattailed base section which includes a domed cavity and a combustion chamber for the solid propellant.

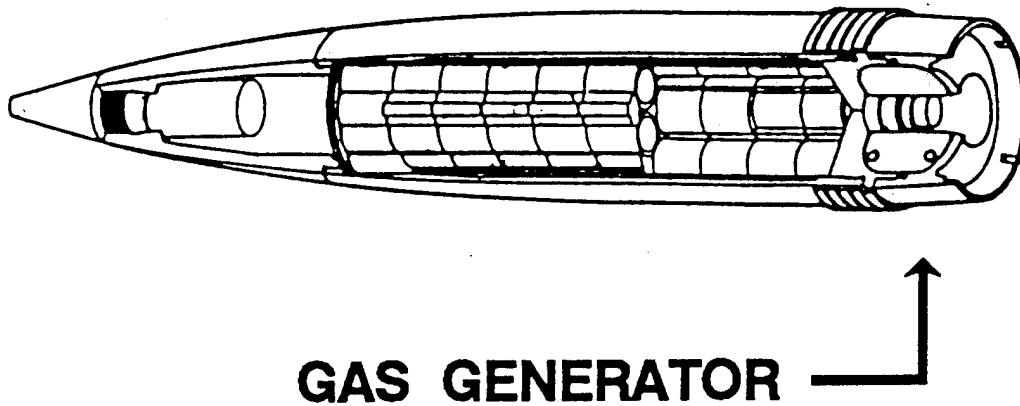


Figure 1. Schematic of M864 base bleed projectile.

The details of this can be seen in the expanded view of the base section shown in Figure 2. Note that the hole in the base is an orifice and not a nozzle design. This is in keeping with the low-speed bleed design as opposed to a rocket-assisted projectile. The shape of the M864 is similar to that of the product-improved M825, which also contains a base cavity (D'Amico 1987). Very limited detailed data exists for the M864, and the effects of both the dome base and the addition of base burn are not well understood.

The majority of base flow calculations had generally modeled the base region as a flat solid surface. Many of the actual configurations have some form of base cavity. General opinion had been that the inclusion of a base cavity or modifications to the interior cavity of a projectile base would have little or no effect on the overall flight performance parameters. Both experimental firings (D'Amico 1987) and computations of the M825 (Sahu and Nietubicz 1989) have shown that this is not the case. Both changes in drag of 2% and changes in lift of approximately 7% have been found.

The Navier-Stokes computational study described here extends the application to include the effect of base burn on the M864 projectile configuration. SRA's Navier-Stokes code, CMINT, has been used

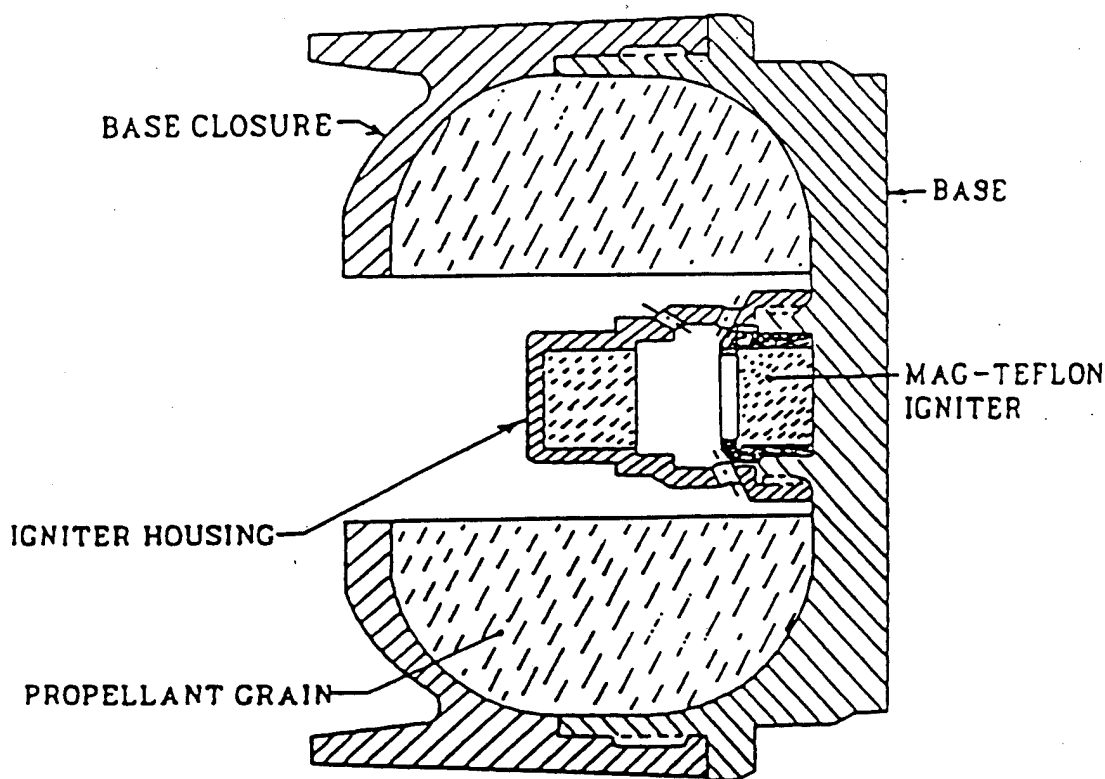


Figure 2. M864 base burn motor.

with an H_2 -CO combustion model to compute the base region flow field. Numerical computations have been completed at $\alpha = 0.0^\circ$ for a Mach number range of $0.8 \leq M \leq 3.0$. A reduction in drag was found first for hot gas injection, with a further reduction in drag due to the wake combustion. Qualitative features of the computed flow fields are presented in the form of temperature contours, species mass fraction contours, and velocity vectors.

2. GOVERNING EQUATIONS AND SOLUTION TECHNIQUE

2.1 Governing Equations. The complete set of time-dependent, ensemble-averaged Navier-Stokes equations with fully coupled species conservation equations is used for the solution of the projectile base burn problem. The numerical technique used is an implicit finite difference scheme. Although the solution of the time-dependent equations is being made, the transient flow is not of interest, and the equations are solved in a time-asymptotic manner.

The governing partial differential equations are written in a strong conservation form using a nonorthogonal, body-fitted, cylindrical coordinate system. Details of the transformation for the full set

of equations are described by Sabnis, Gibeling, and McDonald (1989). The equations presented here are expressed in vector form.

The continuity equation is written as

$$\frac{\partial \rho}{\partial t} + \nabla \cdot (\rho \mathbf{U}) = 0. \quad (1)$$

The momentum conservation equation is

$$\frac{\partial(\rho \mathbf{u})}{\partial t} + \nabla \cdot (\rho \mathbf{U} \mathbf{U}) = -\nabla p + \nabla \cdot \boldsymbol{\tau}, \quad (2)$$

where $\boldsymbol{\tau}$ is the stress tensor (molecular and turbulent) given by

$$\tau_{ij} = 2\mu_{\text{eff}} e_{ij} - \frac{2}{3} \mu_{\text{eff}} \nabla \cdot \mathbf{U} \delta_{ij}, \quad (3)$$

and the rate of strain tensor, e_{ij} , is given by

$$e_{ij} = \frac{1}{2} \left(\frac{\partial u_i}{\partial x_j} + \frac{\partial u_j}{\partial x_i} \right). \quad (4)$$

The effective viscosity, μ_{eff} , is the sum of the molecular and turbulent viscosities

$$\mu_{\text{eff}} = \mu + \mu_T. \quad (5)$$

The turbulent viscosity, μ_T , is obtained from the turbulence model. The turbulence models used for the present study are algebraic and will be discussed at a later time. The energy conservation equation is written in terms of the stagnation enthalpy, h_o , as

$$\frac{\partial(\rho h_o)}{\partial t} + \nabla \cdot (\rho \mathbf{U} h_o) = \frac{\partial p}{\partial t} - \nabla \cdot \mathbf{q} + \nabla \cdot (\boldsymbol{\tau} \cdot \mathbf{U}), \quad (6)$$

where the last term in Equation 6 is the stress work and \mathbf{q} is the heat flux vector,

$$q = -\kappa_{\text{eff}} \nabla T + q_d \quad (7)$$

where κ_{eff} is the effective thermal conductivity and q_d is the interdiffusional energy flux. In the present analysis, κ_{eff} is obtained assuming constant molecular and turbulent Prandtl numbers, Pr and Pr_T ; i.e.,

$$\kappa_{\text{eff}} = \frac{\mu c_p}{Pr} + \frac{\mu_T c_p}{Pr_T} . \quad (8)$$

The interdiffusional energy flux is given by

$$q_d = \sum_{i=1}^{N_s} h_i(T) j_i, \quad (9)$$

where j_i is defined in Equation 12 and $h_i(T)$, the enthalpy of species i per unit mass, is

$$h_i(T) = h_{fi} + \int_{T_f}^T c_{pi}(T') dT' . \quad (10)$$

The species conservation equations are expressed as

$$\frac{\partial(\rho Y_i)}{\partial t} + \nabla \cdot (\rho U Y_i) = -\nabla \cdot j_i + w_i, \quad (11)$$

where Y_i is the mass fraction of species i , w_i is the rate of production of species i due to chemical reaction, and j_i is the diffusional mass flux of species i . Assuming that the diffusion of mass is governed by Fick's law, j_i is given by

$$j_i = -\rho D \nabla \cdot Y_i \quad (12)$$

where D is the diffusion coefficient which is obtained by assuming constant molecular and turbulent Schmidt numbers, Sc and Sc_T ; i.e.,

$$\rho D = \frac{\mu}{Sc} + \frac{\mu_T}{Sc_T} . \quad (13)$$

Finally, for a mixture of perfect gases, the equation of state is

$$p = \rho R T$$

$$R = R_u \sum_{i=1}^{N_s} \frac{Y_i}{W_i} , \quad (14)$$

where R_u is the universal gas constant, W_i is the molecular weight of species i , and N_s is the total number of species in the system. The caloric equation of state relates the temperature and the static enthalpy as

$$h = \sum_{i=1}^{N_s} Y_i h_i(T) . \quad (15)$$

This relation is evaluated using the JANNAF database of polynomial curve fit coefficients for C_{pi} and h_i as functions of T , which are available from NASA Lewis Research Center (Gordon and McBride 1976).

2.2 Turbulence Model. The application of the Baldwin-Lomax algebraic turbulence model to projectile forebody flows has provided excellent results for even the most viscous dominated aerodynamic coefficient such as Magnus force (Sturek and Nietubicz 1992). It has further been applied to wake flows (Sahu, Nietubicz, and Steger 1985; Sahu 1986) and provided reasonable results for the integrated total drag. However, more recent results with a $k-\epsilon$ turbulence model (Sahu 1992) show that when a comparison of base pressure is made with available experimental data, an improved agreement is found over the algebraic model.

The study presented here has used the Baldwin Lomax model for the projectile forebody and a wake mixing model of Chow (1985) for the wake and free shear layer flow behind the projectile base. No

detailed base pressure data is available for the M864, with or without base burn, and a detailed study of turbulence models was not considered at this time. The integrated total drag will be used to determine overall accuracy.

2.3 Chemistry Model. The propellant grain for the M864 is molded in the form of a donut shape to fit within the projectile afterbody. The propellant is split in two, separated by a 3-mm-wide gap. The propellant grain burns both within the inner cylindrical surface and the slot. Details of the propellant formulation were obtained from the manufacturer (Brody 1991). There has been no detailed analysis performed for this combustion process. The NASA Lewis CET86 code (Gordon and McBride 1976) was run and provided combustion products that consisted primarily of H_2 , CO , HCl , CO_2 , H_2O , and N_2 . The mole fractions of these constituents in chemical equilibrium sum to 0.997; hence, there is little error in ignoring the remaining trace species. An equivalent mixture was formulated by Gibeling and Buggeln (1991) to eliminate the HCl where both the heat of combustion and the molecular weight have been matched to those of the original equilibrium combustion products. The composition of the equivalent mixture is given in Table 1.

The reaction rates for the models considered herein are expressed in the Arrhenius form; i.e.,

$$k_f = A T^b \exp\left(-\frac{E_a}{RT}\right)$$

and the backward rate coefficients, k_b , are obtained using the equilibrium constant K_c , where

$$K_c = \frac{k_f}{k_b}.$$

The equilibrium constant is calculated using the Gibbs free energy as described by Vincenti and Kruger (1965). What remains to be specified for the reaction rates to be complete is the temperature. Although the equilibrium temperature can be calculated, assuming the combustion products are in chemical equilibrium, it was specified from data obtained during ground-based (Kayser, Kuzan, and Vazquez 1988) and flight tests (Kayser, Kuzan, and Vazquez 1990) of the M864 projectile. Thermocouples were placed within the combustion chamber, and temperature measurements were taken in a ground fixture where the base was spun and data was taken as a function of spin rate. The ground test indicated an average

Table 1. M864 Propellant Equilibrium Species Concentrations
(Major Species, $T = 1,533$ K, $p = 0.68$ atm)

Species i	CET86 Results		Equivalent Mixture	
	Mole Fraction	M_{wi}	Mole Fraction	Mass Fraction
CO	0.249	28.01	0.265	0.3402
CO ₂	0.069	44.01	0.160	0.3228
HCl	0.136	36.46	0.0	0.0
H ₂	0.261	2.016	0.261	0.0241
H ₂ O	0.197	18.015	0.197	0.1627
N ₂	0.085	28.01	0.117	0.1502
Sum	0.997	(M_w) 21.81	1.000	1.000

chamber temperature of approximately 1,200 K. Similar measurements were obtained from actual flight tests, and data were obtained as a function of range. The temperature measurements from the flight tests indicated an average chamber temperature of approximately 1,500 K. The flight tests are considered to be the more accurate of the two. Therefore, the temperature for the injected gas was assumed to be at 1,533 K.

A series of combustion models for the base burn problem as evaluated by Gibeling and Buggeln (1991). They began by looking at a set contain 23 reactions where the relative importance of each reaction was numerically studied. The final set of 12 modified model reactions determined to adequately model the solid propellant combustion is shown in Table 2 along with the Arrhenius constants for the forward reactions. The backward rates are obtained from k_f and K_c .

2.4 Boundary Conditions. The outer computational boundary was set at approximately two body lengths from the projectile surface. Free-stream conditions were then imposed along the outer boundary. Viscous boundary conditions of no slip were used at the wall and projectile base. The normal momentum equation is solved at the wall using a zero normal pressure gradient and zero gradient for species mass fractions. The free-flight wall temperature is specified at $T_w = 294$ K, and using the time-lagged pressure,

Table 2. Carbon Monoxide Oxidation Mechanism (Gibeling and Buggeln 1991) With Rate Constant:
 $k_f = A T^b \exp(-E_a/RT)^a$

Reaction					A	b	E_a (kJ/mole)
1.	H	+ O ₂	→ OH	+ O	1.2×10^{17}	-0.91	69.1
2.	H ₂	+ O	→ OH	+ H	1.5×10^7	2.00	31.6
3.	O	+ H ₂ O	→ OH	+ OH	1.5×10^{10}	1.14	72.2
4.	OH	+ H ₂	→ H ₂ O	+ H	1.0×10^8	1.60	13.8
5.	O	+ H	+ M → OH	+ M	1.0×10^{16}	0.00	0.0
6.	O	+ O	+ M → O ₂	+ M	1.0×10^{17}	-1.00	0.0
7.	H	+ H	+ M → H ₂	+ M	9.7×10^{16}	-0.60	0.0
8.	H ₂ O	+ M	→ H	+ OH + M	1.6×10^{17}	0.00	478.0
9.	O ₂	+ H ₂	→ OH	+ OH	7.94×10^{14}	0.00	187.0
10.	CO	+ OH	→ CO ₂	+ H	4.4×10^6	1.50	-3.1
11.	CO	+ O	+ M → CO ₂	+ M	5.3×10^{13}	0.00	-19.0
12.	CO	+ O ₂	→ CO ₂	+ O	2.5×10^{12}	0.00	200.0

^a Dimensions of k_f are $[\text{cm}^3 / \text{mole}]^{m-1} \text{sec}^{-1}$ where m is the reaction order; T is in Kelvin. Reverse rate constants k_b are obtained from k_f and the equilibrium constant K_c .

the density at the wall is determined. The base bleed boundary conditions require a specification of the mass injection rate I , where

$$I = \frac{m_i}{\rho_\infty U_\infty A_{\text{base}}}$$

and m_i is the injection mass flow rate. With the mass injection specified, the Mach number at the base bleed hole can be determined from

$$M_j^2 = \frac{1}{\gamma - 1} \left\{ -1 + \sqrt{1 + 2(\gamma - 1) \frac{T_{oj}}{T_\infty} \left[\text{IM}_\infty \frac{P_\infty A_b}{P_j A_j} \right]^2} \right\} \quad (19)$$

where subscripts b and j refer to conditions at the bleed orifice. The computed pressure and flow field variables from the previous time step are used. With the bleed gas stagnation pressure and static

temperature then determined from isentropic relations, the density for the bleed conditions is obtained. This formulation was first developed and applied by Danberg and Nietubicz (1992). All cases presented here have used an injection parameter, $I = 0.0022$, which is somewhat lower than the average value. Data deduced from flight tests of the M864 (Lieske and Danberg 1992) indicate an average mass injection value of $I = 0.006$. The stagnation temperature of the injected gas was 1,533 K. At the downstream boundary, an outflow condition of first derivative extrapolation was used.

2.5 Solution Technique. The set of equations described earlier was solved using a linearized block implicit (LBI) algorithm and an ADI approximate factorization technique as developed by Briley and McDonald (1977). Centered spatial differencing is used, and suppression of high-frequency oscillations due to severe flow field gradients is achieved using an adjustable artificial dissipation. Steady state results are achieved by advancing the solution in time. A spatially varying time step was used to accelerate convergence to a steady solution. The solution of the reacting set of equations required further time conditioning, which was achieved by using a time step scaling based on the chemical production source terms in the species equations (Eklund, Drummond, and Hassan 1990). A more complete description of the solution technique is given by and representative applications may be found in Briley et al. (1991).

The code used for the results presented here is a reacting flow version of CMINT. This code was extended, under contract, to include the base boundary conditions described earlier and then applied to a flat base projectile. The analysis and theory are described in Gibeling and Buggeln (1992a). A user's guide for this code, CMINT Version 5.04-BRL (Gibeling and Buggeln 1992b), has also been developed.

2.6 Computational Grid. As with most all artillery shells, the M864 has a groove in the nose fuze and has a rotating band. The computational model used is shown in Figure 3 and does not include these details. The flat nose and fuze ogive, however, have been modeled. The general shape of the internal base cavity is shown as a dotted line on the boattail section. The base burn motor is located internally with the exhaust port centered on the model axis. The initial body point distribution was provided using an interactive design program. Each grid section (projectile body and base) was then obtained using a hyperbolic grid generation program (Nietubicz, Heavey, and Steger 1982). Due to the extreme concavity of the M864 base section, both smoothing and grid cell averaging were required to eliminate grid line crossing. Details of the smoothing procedure as well as a description of an interactive version of the hyperbolic grid generator can be found in Ferry and Nietubicz (1992).

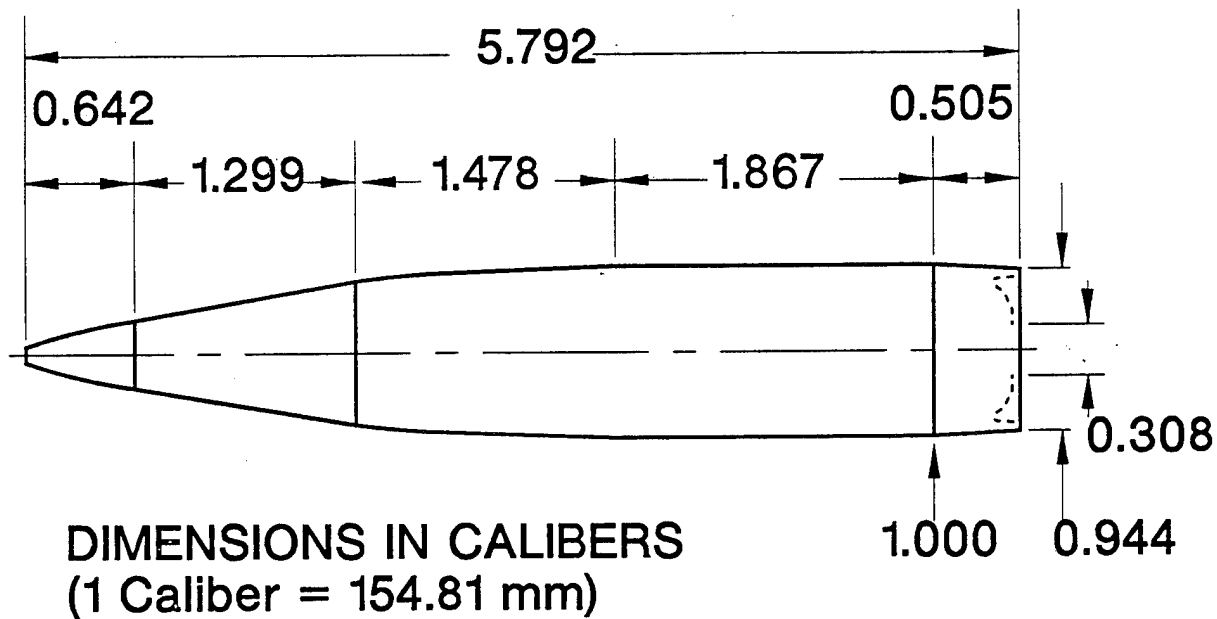


Figure 3. M864 computational model.

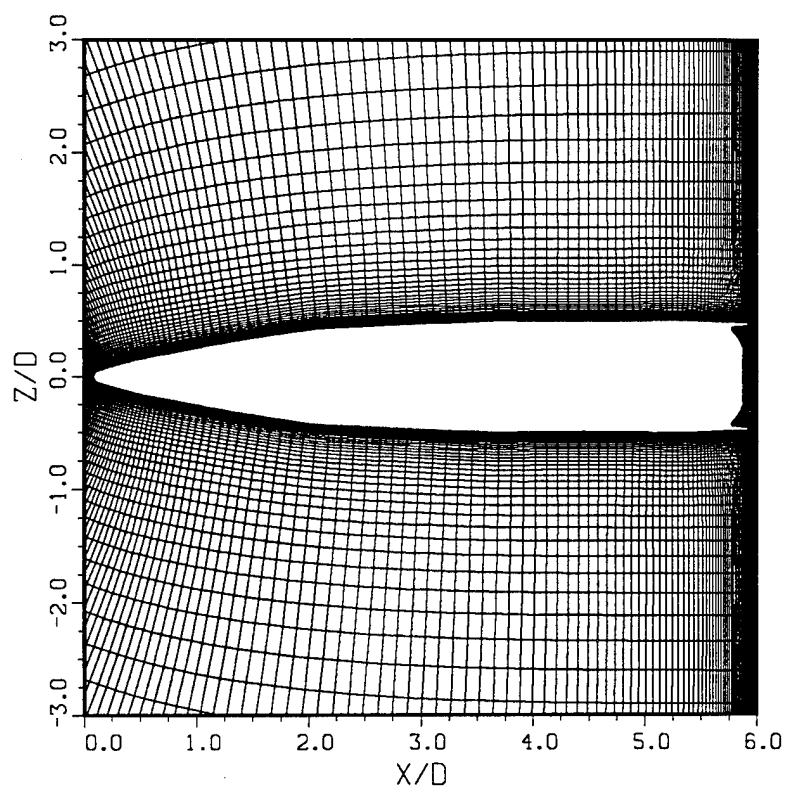


Figure 4. Computational grid near projectile surface.

Figure 4 shows the computational grid generated in the vicinity of the projectile body. It consists of 145 longitudinal points up to the base corner and 90 points in the normal direction. The near-wall grid resolution in the transverse direction (i.e., $\nabla r/D$) was 2×10^{-5} to provide sublayer resolution. Although this spacing provided a few points within the viscous sublayer, subsequent results have shown that a near-wall resolution of $(\nabla r/D) 5 \times 10^{-5}$ is required for more accurate viscous results.

Figure 5 shows the base region grid. This grid section contains 90 points radially from the centerline to the base corner, and 90 points from the corner to the outer boundary. There are 20 points in the injection region, which extends from the centerline to a radius of 0.15 caliber. From the base corner to the downstream outflow boundary, there are 150 points. The large number of points in the base region and the concentration in the near-wake region were required for the reacting flow cases.

2.7 Results. The primary goals of this research effort were to apply the CMINT code to the M864 projectile for a series of Mach numbers, determine the effect of combustion in the wake region, and compare the results with the available experimental data. To achieve these goals, computations were performed for a Mach number range of $0.8 \leq M \leq 3.0$, $\alpha = 0.0^\circ$. All cases were run for atmospheric conditions with $T_\infty = 294$ K. The bleed gas temperature, T_j , was based on experimental flight data (Stahle, Hubbart, and Walterick 1982) and set to $T_j = 1,533$ K. As discussed previously, the mass injection, I , was set to 0.0022.

The computations were performed by running a full projectile case with no base burn (inert). After convergence, a starting profile was selected on the boattail, approximately 1/2 caliber from the base. This data was used for subsequent base combustion runs. Each case ran approximately 2,000 steps until a converged solution was obtained. The data are presented in the form of Mach contours, temperature contours, and species mass fraction contours. Also, the drag force coefficient has been determined and compared with results obtained from a trajectory simulation program.

Temperature contours are initially compared for a case with hot gas injection (see Figure 6) and H_2 -CO combustion (Figure 7). Hot air injection has a significant effect on the size and shape of the recirculation zone. This was shown by Nietubicz and Sahu (1986) where injection of air at 1,200 K was shown to move the recirculation zone downstream approximately 1/2 caliber. With the addition of burning in the wake, the additional temperature increase can be seen in Figure 7 to extend further into the

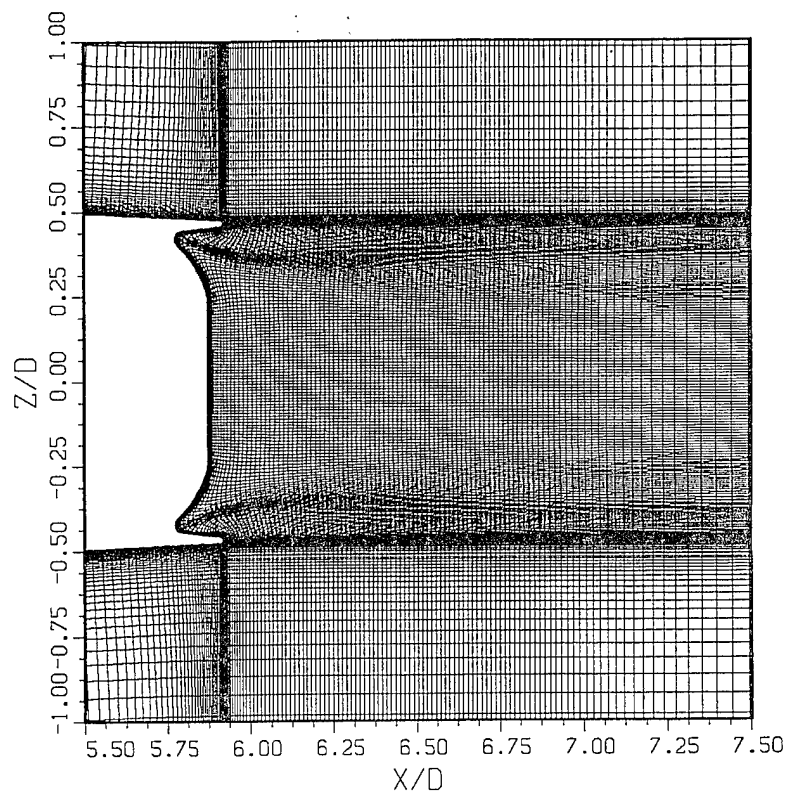
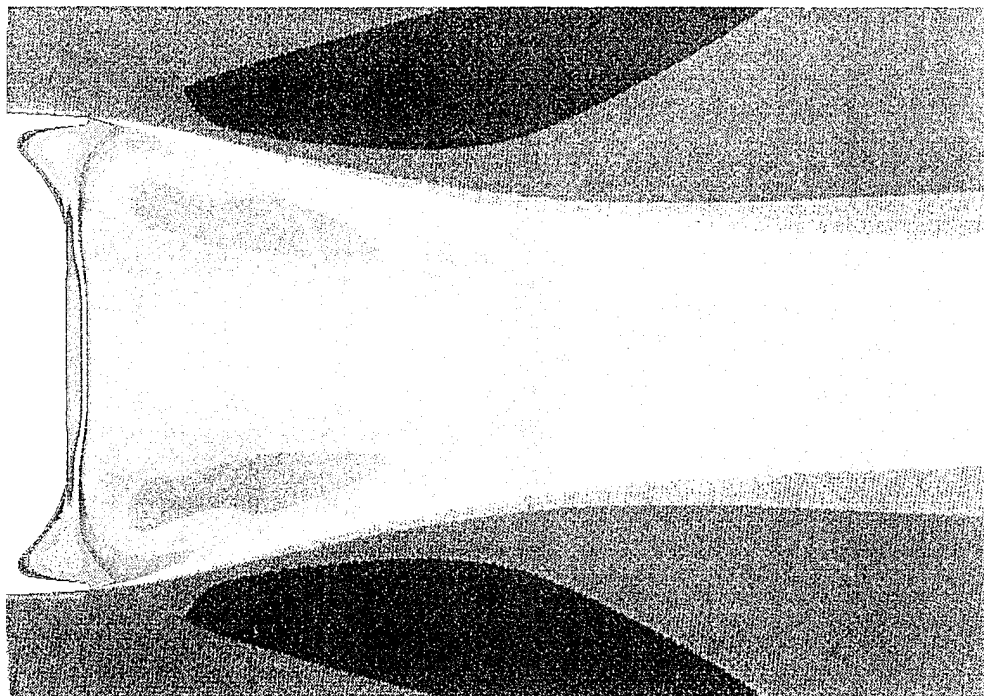


Figure 5. M864 base region grid.



CONTOUR LEVEL

0.80000
1.00000
1.20000
1.40000
1.60000
1.80000
2.00000
2.20000
2.40000
2.60000
2.80000
3.00000
3.20000
3.40000
3.60000
3.80000
4.00000
4.20000
4.40000
4.60000
4.80000
5.00000
5.20000
5.40000

Figure 6. Temperature contours, hot air injection, $M_\infty = 2.0$, $T = 1,533$ K.

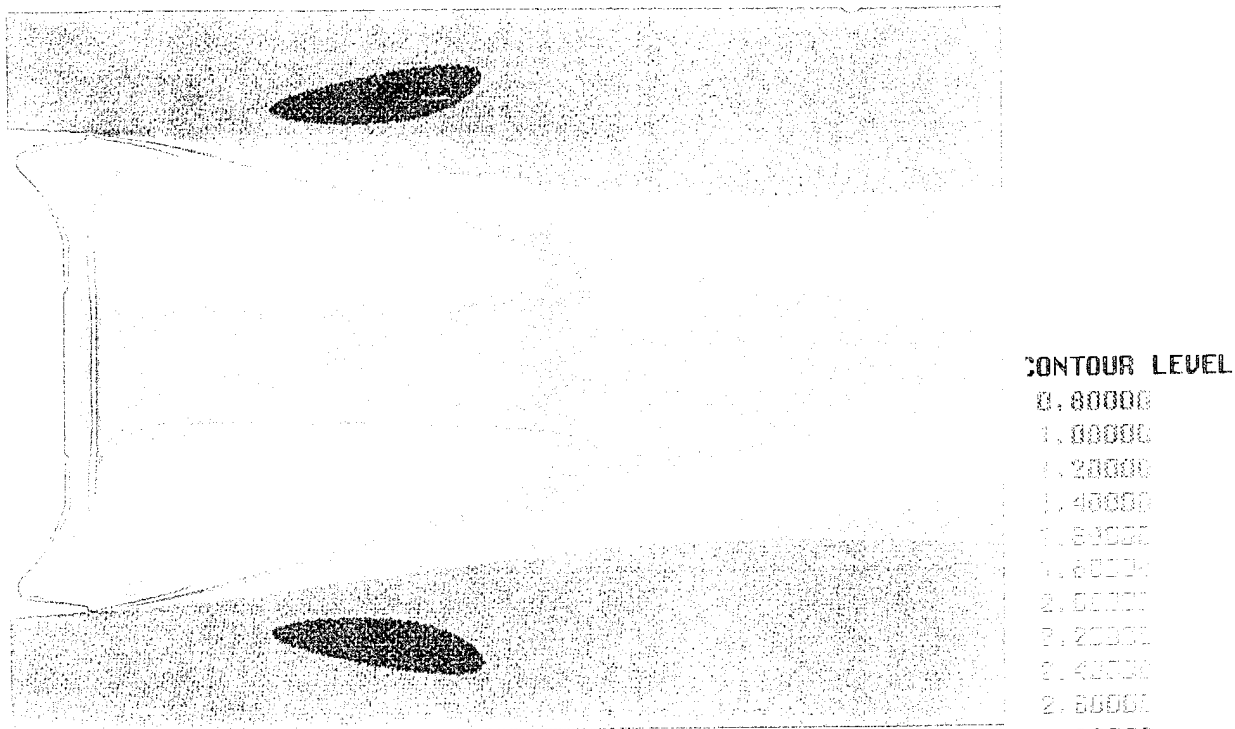


Figure 7. Temperature contours, H_2 -CO injection, $M_\infty = 2.0$, $T_j = 1,533$ K.

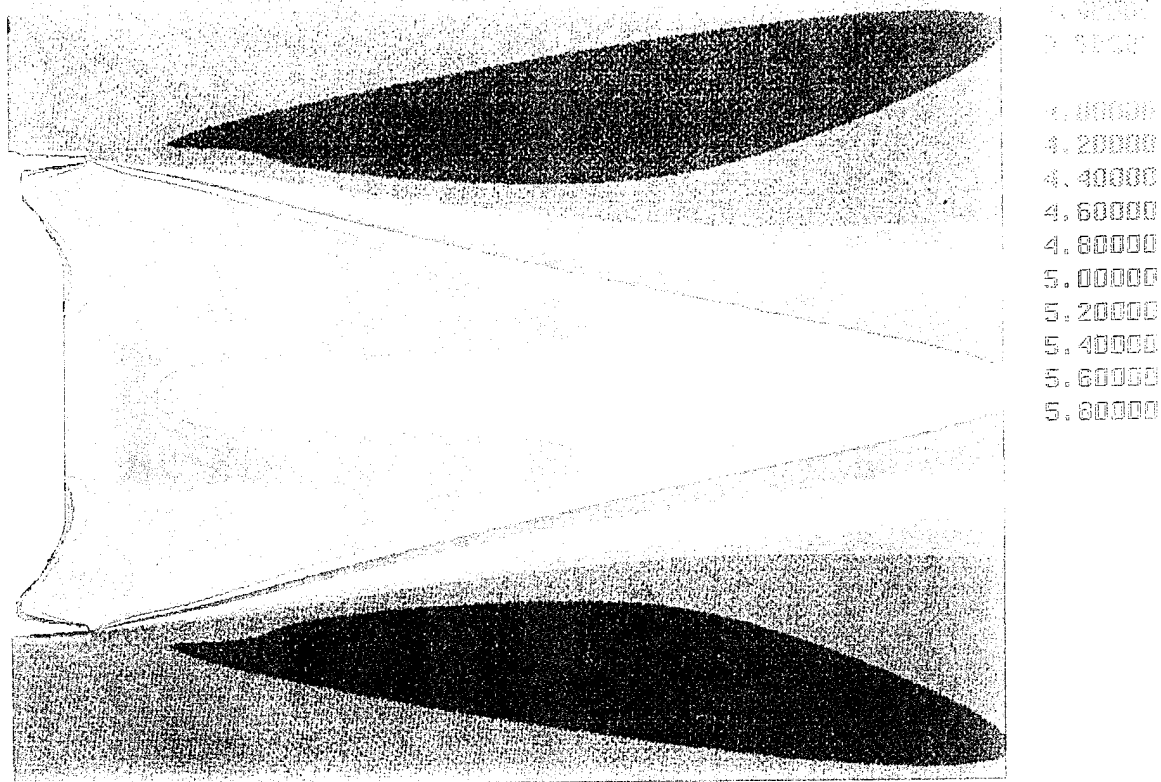


Figure 8. Temperature contours, H_2 -CO injection, $M = 3.0$.

recirculation zone than for the hot gas case (Figure 6). Additionally, the high temperature is seen to exist in the concave portion of the M864 base, very near the base corner. This increase in the recirculation zone causes the expansion at the base corner to weaken even further than the hot gas case and thus raise the base pressure, causing the drag to decrease. Temperature contours are shown in Figure 8 for Mach = 3.0. The base corner region is shown to be at an elevated temperature with the effect extending well in to the near-wake region. This increased temperature results from the combustion of H_2 -CO in the wake. A comparison of the temperature contours for the $M = 1.5$ and $M = 3.0$ is shown in Figure 9. The increased temperature is again distributed within the near-wake region, however the $M = 1.5$ shows generally lower values overall.

Additional evidence of base burning can be seen from the species mass fraction contours shown in Figure 10 for CO. Both CO and H_2 are the primary species which control the combustion process in the wake. The contours show a strong mass fraction level of CO very near the bleed hole and extending up to the base corner. These high, fuel-rich concentration areas give rise to active combustion zones, which was indicated by the elevated temperature in those regions. Figure 11 compares the CO mass fraction for the Mach 1.5 and 3.0 case. Here the distribution in the wake is about the same for both cases, with the $M = 1.5$ showing the higher mass fraction level more near the bleed hole.

Mach contours are presented in Figure 12 for $M_\infty = 3.0$ and indicate the low-speed wake flow and size of the recirculation region. The stand-off distance of the recirculation region decreases as the free-stream Mach number increases. This can be seen in the comparison plot of Figure 13 where Mach contours for both the $M_\infty = 1.5$ and $M_\infty = 3.0$ case are shown. However, the effect of the increased temperature due to combustion minimizes this decrease. The effect on the base pressure is directly related to this change. The injection of gas into the base region and subsequent burning will move the recirculation downstream. This process will result in a downstream shift in the wake closure location and a reduced expansion at the base corner, which implies an increase in base pressure.

The base pressure is shown in Figure 14 as a function of radial position for all the Mach numbers computed. The base pressure is seen to be constant from the edge of the bleed orifice ($r/D = 0.14$) to the base corner. Across the bleed orifice, the pressure is seen to increase. Currently there is no base pressure data available for the M864 with base burn. Recent comparisons of computed base pressure by

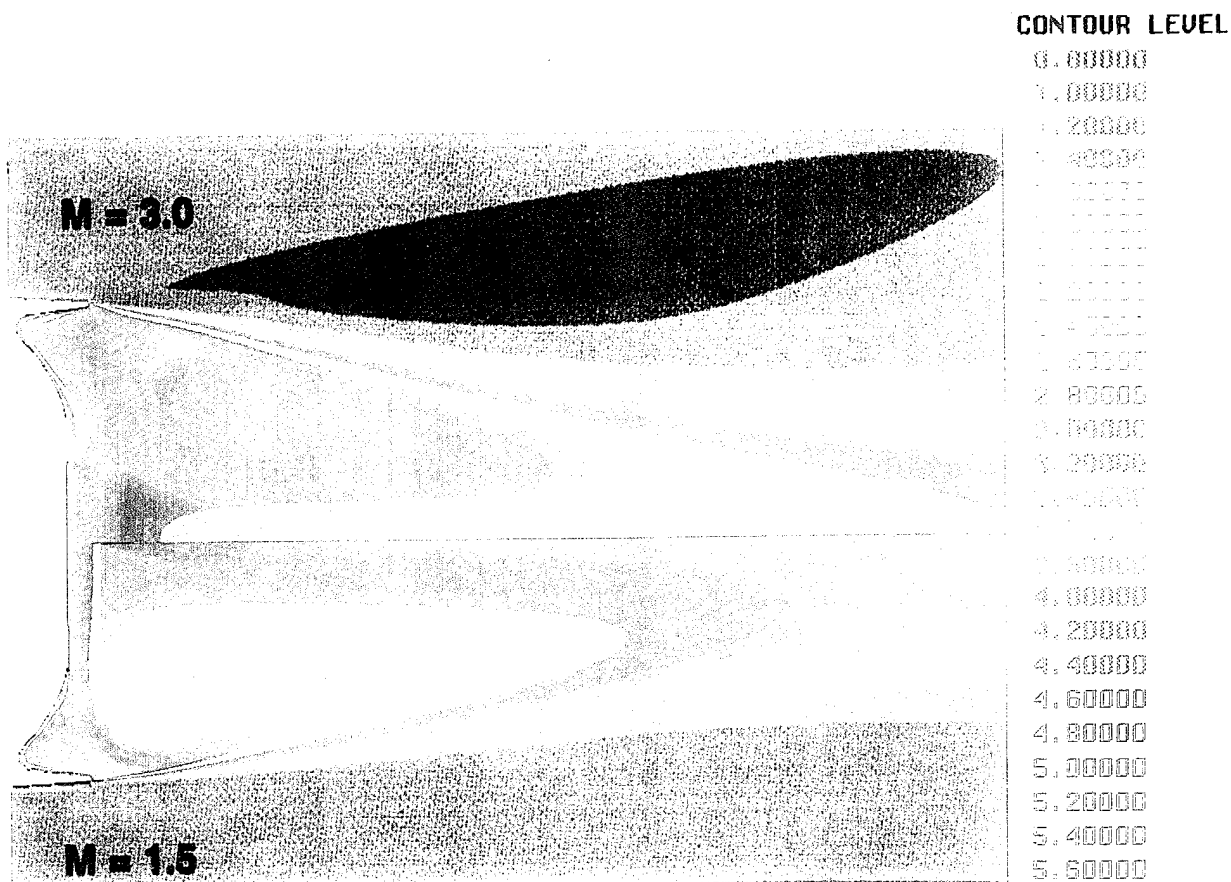


Figure 9. (U) Comparison of temperature contours, $M = 1.5$ (bottom) and $M = 3.0$ (top).

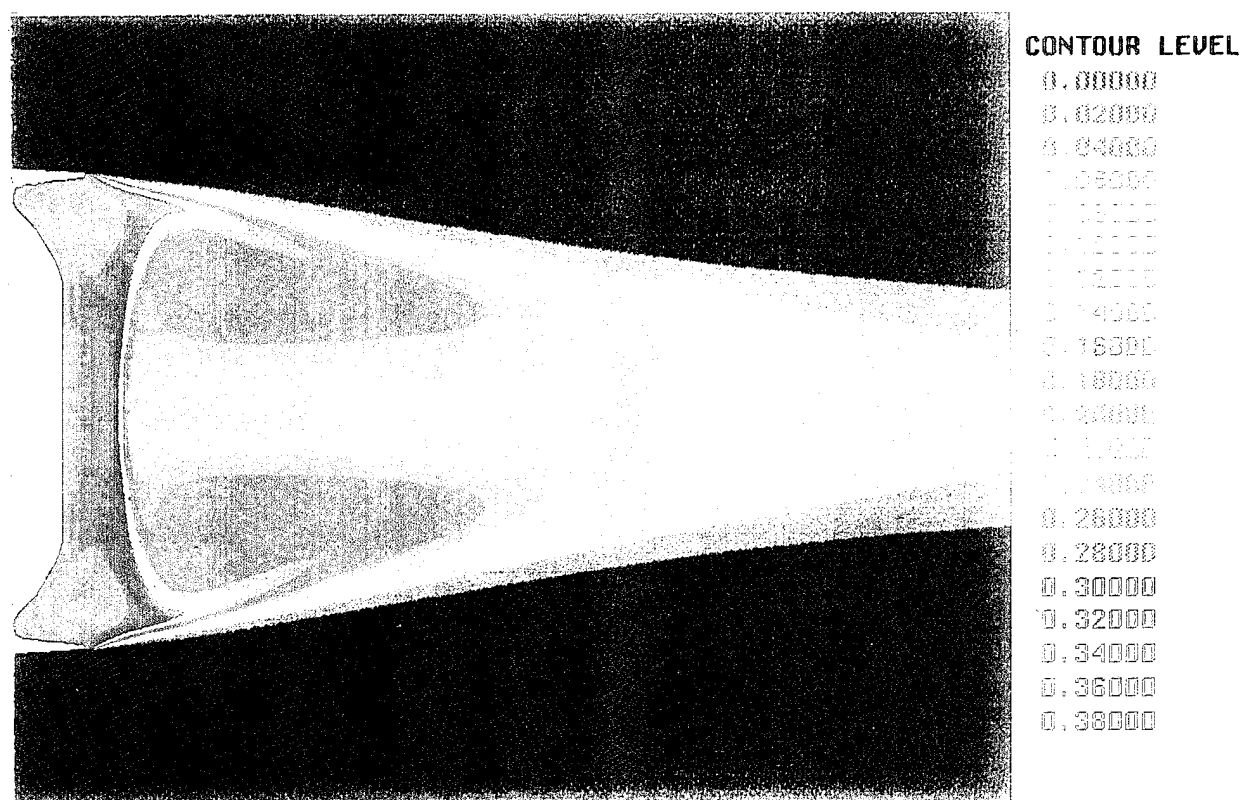


Figure 10. Species mass fraction contours for CO, $M = 3.0$.

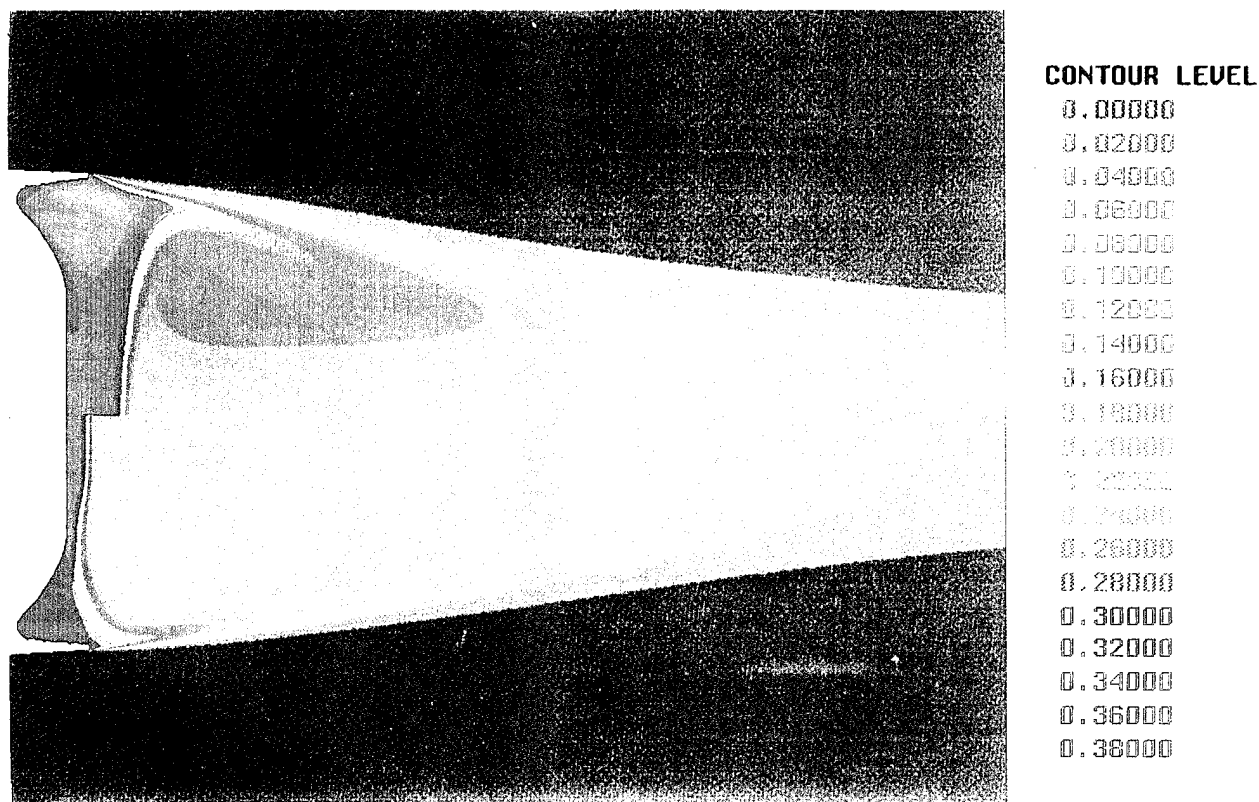


Figure 11. Comparison of species mass fraction for CO, $M = 1.5$ (bottom) and $M = 3.0$ (top).

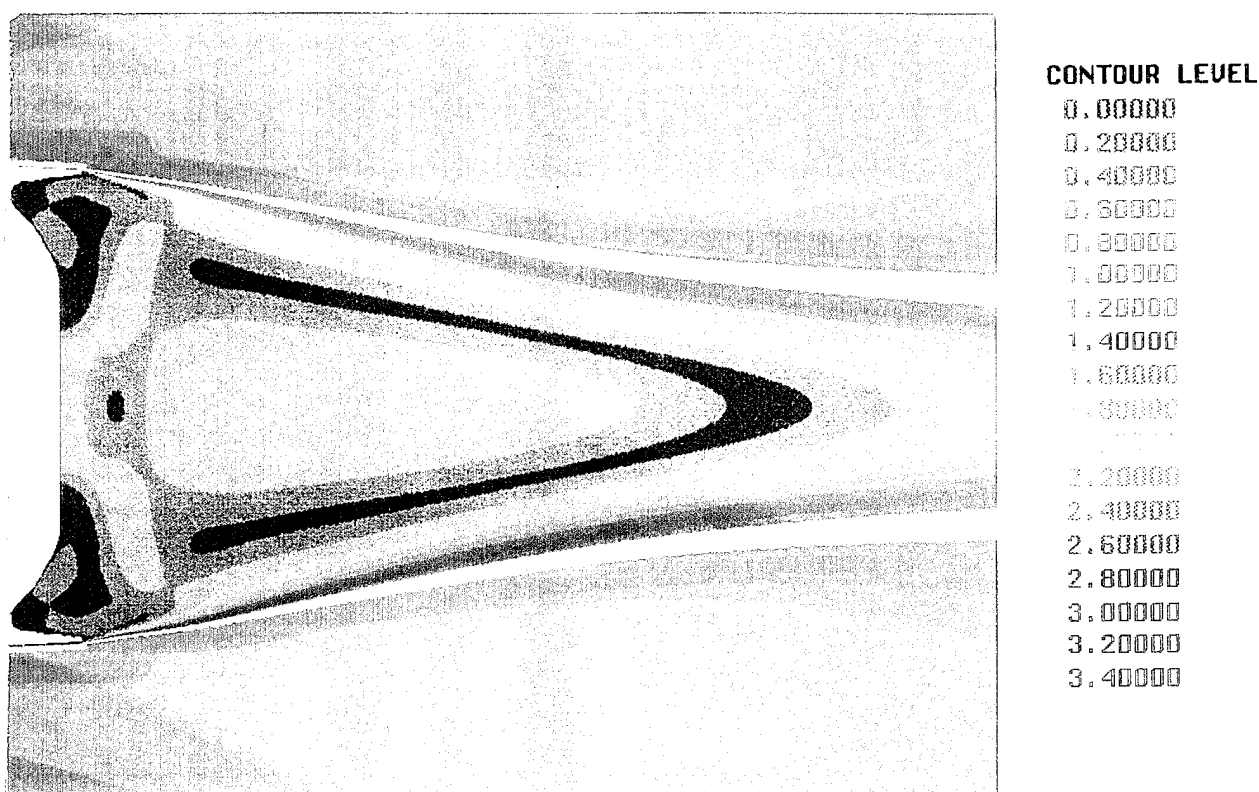


Figure 12. Mach contours, $M_\infty = 3.0$.

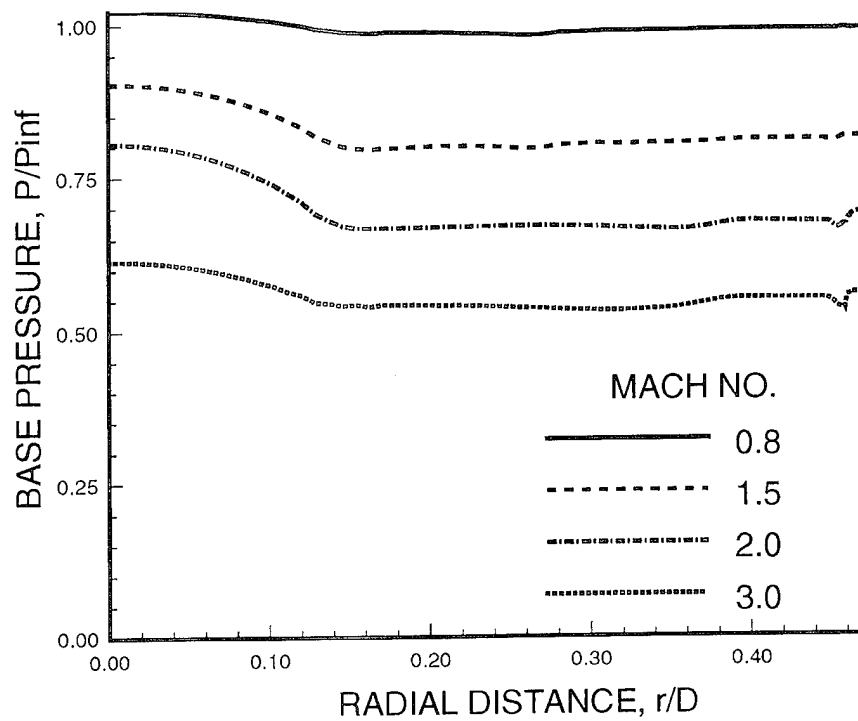


Figure 13. Comparison of Mach contours, $M_{\infty} = 1.5$ (bottom) and $M_{\infty} = 3.0$ (top).

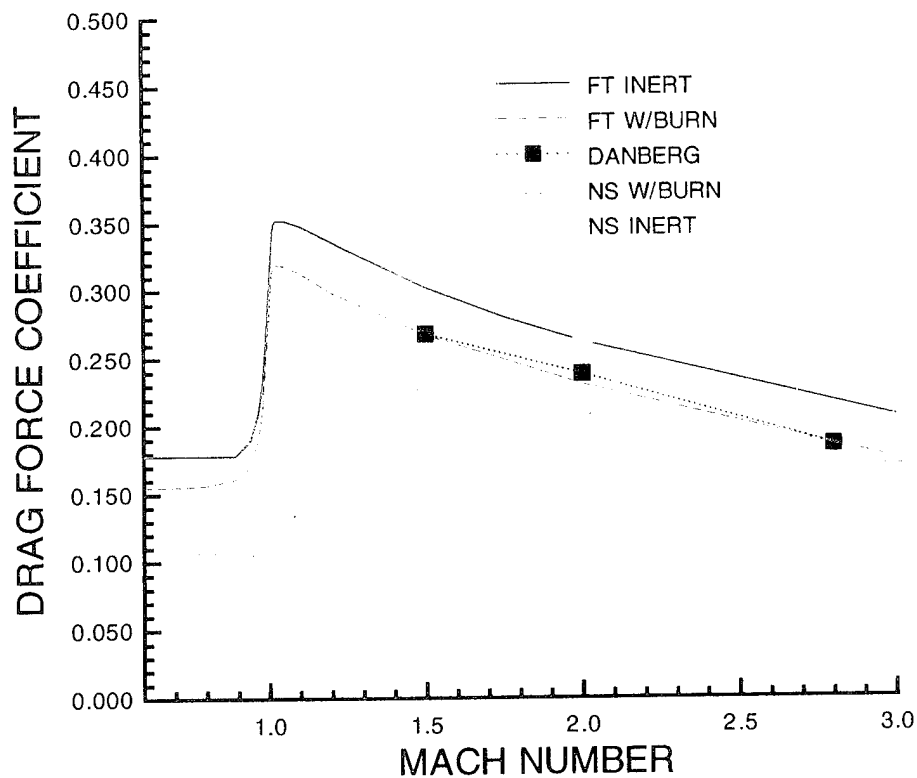


Figure 14. Base pressure vs. radial position.

Sahu (1992) with data from the University of Illinois for a nonbleed case show a constant base pressure for the supersonic condition tested.

Given the lack of detailed experimental data for the M864, comparisons have been made for the zero yaw drag values, which can be obtained from the computations and from experimental flight tests. Lieske and Danberg (1992) have modified a point mass trajectory model for rocket-assisted projectiles to include the effect of base burn. The modification models the change in base drag due to changes in the base pressure caused by the hot gas injection. The model is adjusted with a drag reduction factor and constants determined from actual flight tests of the M864. Since the model has been adjusted by flight tests data and the computations have been performed for the same configuration, a comparison of the zero yaw drag under base burn conditions can be made. The model was run for the same conditions as those computed (i.e., atmospheric pressure and temperature, $I = 0.0022$ and $T_j = 1,533$ K).

A plot of the total drag force coefficient obtained from the trajectory model (Lieske and Danberg 1992; Lieske 1992) is shown in Figure 15. The model predictions for both an inert and base burn case are shown by the solid and dashed lines, respectively. The results from the Navier-Stokes computation with combustion are shown in the solid symbols. Also shown as a dotted line with open squares are the results from Danberg's engineering model (Danberg and Nietubicz 1992), which was run for the same conditions as the computations. This model combines the solid motor burn performance, the effect of hot mass injection on drag, and a trajectory model. The comparison is shown to be in some agreement at the higher Mach numbers, but falls off at the lower values. This is especially true at the subsonic condition of Mach 0.8. The underprediction of the total drag for the subsonic case has also been found without base burn or base bleed. Work in the areas of turbulence modeling, different algorithms, and adaptive gridding are being used to help resolve this problem area. The inert results have in the past been generally good for supersonic conditions, and a sample result is shown as a solid triangle in Figure 13. The agreement with the trajectory model predictions is shown to be very good.

Additional work needs to be accomplished for the base bleed/base burn configurations both on an experimental and computational basis. Detailed pressure measurements on the base of the M864 would be valuable, as well a better description of the fuel-rich exhaust of the M864 base burn motor.

3. SUMMARY

Computations were performed for the M864 base burn projectile across a Mach number range of $0.8 \leq M \leq 3.0$. A modified version of the SRA CMINT code was used with a combustion model containing 6 species and 13 reactions. The results have shown an increased temperature in the near-wake region of all cases and a decrease in the base drag over the hot injection case. The computed results were compared to a trajectory simulation based on the flight performance of a large number of M864 rounds. The comparison was fair at the higher Mach number, but falls off substantially in the subsonic region. Base pressure data is limited in the subsonic region for projectiles both with and without base bleed/base burn. This type of data would be valuable in accessing the reasons for the underprediction of base drag in subsonic flow.

4. REFERENCES

- Baker, W. T., T. Davis, and S. E. Matthews. "Reduction of Drag of a Projectile in a Supersonic Stream by the Combustion of Hydrogen in the Turbulent Wake." APL Report CM-637, Applied Physics Laboratory, Johns Hopkins University, 1951.
- Briley, W. R., and H. McDonald. "Solution of the Multidimensional Compressible Navier-Stokes Equations by a Generalized Implicit Method." Journal of Comp. Physics, vol. 24, pp. 372-397, 1977.
- Briley, W. R., D. V. Roscoe, H. J. Gibeling, R. C. Buggeln, J. S. Sabnis, P. D. Johnson, and F. W. Huber. "Computation of Flow Past a Turbine Blade With and Without Tip Clearance." ASME Paper No. 91-GT-56, June 1991.
- Brody, F. Private communications. U.S. Army Research, Development, and Engineering Center.
- Chow, W. L. "Improvement on Numerical Computation of the Thin-Layer Navier-Stokes Equation—With Emphasis on the Turbulent Base Pressure of a Projectile in Transonic Flight Condition." Delivery Order 1713, Contract No. DAAG29-81-D-0100, November 1985.
- D'Amico, W. P., J. Wall, and J. Kochenderfer. "Aerodynamic Testing of an All-Steel Generic Base for ICM-Type Projectiles." Proceedings of the 10th International Symposium on Ballistics, San Diego, CA, 27-29 October 1987.
- Danberg, J. E. "Analysis of the Flight Performance of the 155-mm M864 Base Burn Projectile." BRL-TR-3083, U.S. Army Ballistic Research Laboratory, Aberdeen Proving Ground, MD, April 1990.
- Danberg, J. E. "XM971 Base Bleed Parameter Study." BRL-MR-3948, U.S. Army Ballistic Research Laboratory, Aberdeen Proving Ground, MD, October 1991.
- Danberg, J. E., and C. J. Nietubicz. "Predicted Flight Performance of Base Bleed Projectiles." Journal of Spacecraft and Rockets, vol. 29, no. 3, pp. 366-372, May-June 1992.
- Eklund, D. R., J. P. Drummond, and H. A. Hassan. "Calculation of Supersonic Turbulent Reacting Coaxial Jets." AIAA Journal, vol. 28, no. 9, pp. 1633-1641, 1990.
- Ferry, E. N., Jr., and C. J. Nietubicz. "Interactive Hyperbolic Grid Generation for Projectile CFD." BRL-MR-3971, U.S. Army Ballistic Research Laboratory, Aberdeen Proving Ground, MD, May 1992.
- Gibeling, H. J., and R. C. Buggeln. "Reacting Flow Models for Navier-Stokes Analysis of Projectile Base Combustion." AIAA Paper No. 91-2077, June 1991.
- Gibeling, H. J., and R. C. Buggeln. "Projectile Base Bleed Technology Part I: Analysis and Results." ARL-CR-2, U.S. Army Research Laboratory, Aberdeen Proving Ground, MD, November 1992a.
- Gibeling, H. J., and R. C. Buggeln. "Projectile Base Bleed Technology Part II: User's Guide CMINT Computer Code Version 5.04-BRL." ARL-CR-3, U.S. Army Research Laboratory, Aberdeen Proving Ground, MD, November 1992b.

- Gordon, S., and B. J. McBride. "Computer Program for Calculation of Complex Chemical Equilibrium Compositions, Rocket Performance, Incident and Reflected Shocks, and Chapman-Jouguet Detonations." NASA SP-273, interim revision, March 1976.
- Kayser, L. D., J. D. Kuzan, and D. N. Vazquez. "Ground Testing for Base-Burn Projectile Systems." BRL-MR-3708, U.S. Army Ballistic Research Laboratory, Aberdeen Proving Ground, MD, November 1988 (AD 201107).
- Kayser, L. D., J. D. Kuzan, and D. N. Vazquez. "Flight Testing for a 155-mm Base Burn Projectile." BRL-MR-3830, U.S. Army Ballistic Research Laboratory, Aberdeen Proving Ground, MD, April 1990 (AD 201107).
- Lieske, R. F. Private communication. U.S. Army Ballistic Research Laboratory, Aberdeen Proving Ground, MD, March 1992.
- Lieske, R. F., and J. E. Danberg. "Modified Point Mass Trajectory Simulation for Base-Burn Projectiles." BRL-TR-3321, U.S. Army Ballistic Research Laboratory, Aberdeen Proving Ground, MD, March 1992.
- Murthy, S. N. B., and J. R. Osborn. "Base Flow Phenomena With and Without Injection: Experimental Results, Theories and Bibliography." AIAA Progress in Astronautics and Aeronautics, vol. 40, pp. 7-210, 1976.
- Murthy, S. N. B., J. R. Osborn, A. W. Barrows, and J. R. Ward, editors. Aerodynamics of Base Combustion, AIAA Progress in Astronautics and Aeronautics, vol. 40, 1976.
- Nietubicz, C. J., K. R. Heavey, and J. L. Steger. "Grid Generation Techniques for Projectile Configurations." Proceedings of the 1982 Army Numerical Analysis and Computers Conference, ARO Report 82-3, February 1982.
- Nietubicz, C. J., and J. Sahu. "Navier-Stokes Computations of Base Bleed Projectiles." Paper No. II-2, First International Symposium on Special Topics in Chemical Propulsion: Base Bleed, Athens, Greece, November 1988.
- Sabnis, J. S., H. J. Gibeling, and H. McDonald. "Navier-Stokes Analysis of Solid Propellant Rocket Motor Internal Flows." Journal of Propulsion and Power, vol. 5, no. 6, pp. 657-664, 1989.
- Sahu, J. "Supersonic Flow Over Cylindrical Afterbodies With Base Bleed." BRL-TR-2742, U.S. Army Ballistic Research Laboratory, Aberdeen Proving Ground, MD, June 1986. Also, AIAA Paper No. 86-0487.
- Sahu, J. "Numerical Computations of Supersonic Base Flow With Special Emphasis on Turbulence Modeling." AIAA Paper No. 92-4352-CP, August 1992.
- Sahu, J., and C. J. Nietubicz. "Three Dimensional Flow Calculations for a Projectile With Standard and Dome Bases." SAE Paper No. 892291, September 1989.
- Sahu, J., C. J. Nietubicz, and J. L. Steger. "Navier-Stokes Computations of Projectile Base Flow With and Without Base Injection." AIAA Journal, vol. 23, no. 9, pp. 1348-1355, 1985.

Strahle, W. C., J. E. Hubbart, and R. Walterick. "Base Burning Performance at Mach 3." AIAA Journal, vol. 20, no. 7, pp. 986–991, 1982.

Sturek, W., and C. Nietubicz. "Recent Applications of CFD to the Aerodynamics of Army Projectiles at the U.S. Army Ballistic Research Laboratory." AIAA Paper No. 92-4349-CP, August 1992.

Vincenti, W. G., and C. H. Kruger, Jr. Introduction to Physical Gas Dynamics, New York: Wiley, 1965.

INTENTIONALLY LEFT BLANK.

<u>NO. OF COPIES</u>	<u>ORGANIZATION</u>
2	ADMINISTRATOR DEFENSE TECHNICAL INFO CTR ATTN DTIC DDA CAMERON STATION ALEXANDRIA VA 22304-6145
1	DIRECTOR US ARMY RESEARCH LAB ATTN AMSRL OP SD TA 2800 POWDER MILL RD ADELPHI MD 20783-1145
3	DIRECTOR US ARMY RESEARCH LAB ATTN AMSRL OP SD TL 2800 POWDER MILL RD ADELPHI MD 20783-1145
1	DIRECTOR US ARMY RESEARCH LAB ATTN AMSRL OP SD TP 2800 POWDER MILL RD ADELPHI MD 20783-1145
	<u>ABERDEEN PROVING GROUND</u>
5	DIR USARL ATTN AMSRL OP AP L (305)

NO. OF
COPIES ORGANIZATION

1 HQDA
ATTN SARD TR MS K KOMINOS
PENTAGON
WASHINGTON DC 20310-0103

1 HQDA
ATTN SARD TR DR R CHAIT
PENTAGON
WASHINGTON DC 20310-0103

3 COMMANDER
US ARMY ARDEC
ATTN SMCAR AET A
H HUDGINS
S KAHN
J GRAU
PICATINNY ARSENAL NJ 07806-5000

1 COMMANDER
US ARMY MISSILE COMMAND
ATTN AMSMI RD SS AT B WALKER
REDSTONE ARSENAL AL 35898-5010

1 COMMANDER
US NAVAL SURFACE WARFARE CTR
DAHLGREN DIVISION
ATTN DR F MOORE
DAHLGREN VA 22448

3 COMMANDER
NAVAL SURFACE WARFARE CTR
ATTN CODE R44
DR F PRIOLO
DR A WARDLAW
K24 B402 12 DR W YANTA
WHITE OAK LABORATORY
SILVER SPRING MD 20903-5000

3 AIR FORCE ARMAMENT LABORATORY
AIR FORCE SYSTEMS COMMAND
ATTN AFATL FXA
DR L B SIMPSON
DR DAVID BELK
DR G ABATE
EGLIN AFB FL 32542-5434

NO. OF
COPIES ORGANIZATION

1 USAF WRIGHT AERONAUTICAL
LABORATORIES
ATTN AFWAL FIMG DR J SHANG
WPAFB OH 45433-8553

3 DIRECTOR
NATL AERONAUTICS & SPACE ADMN
LANGLEY RESEARCH CTR
ATTN TECH LIBRARY
DR M J HEMSCH
DR J SMITH
LANGLEY STATION
HAMPTON VA 23665

3 DIRECTOR
NATL AERONAUTICS & SPACE ADMN
AMES RESEARCH CTR
ATTN MS 227 8 L SCHIFF
MS 258 1
T HOLST
D CHAUSSEE
MOFFETT FIELD CA 94035

1 MASSACHUSETTS INST OF TECHLGY
ATTN TECHNICAL LIBRARY
77 MASSACHUSETTS AVE
CAMBRIDGE MA 02139

2 DIRECTOR
SANDIA NATL LABORATORIES
ATTN DR W OBERKAMPF
DR F BLOTTNER
DIVISION 1554
PO BOX 5800
ALBUQUERQUE NM 87185

2 VRA INC
ATTN DR C LEWIS
DR B A BHUTTA
PO BOX 50
BLACKSBURG VA 24060

1 SCIENCE APPLICATIONS INC
COMPUTATIONAL FLUID DYNAMICS DIV
ATTN DR D W HALL
994 OLD EAGLE SCHOOL RD
SUITE 1018
WAYNE PA 19087

NO. OF
COPIES ORGANIZATION

6 ALLIANT TECHSYSTEMS INC
ATTN J BODE
C CANDLAND
L OSGOOD
R BURETTA
R BECKER
M SWENSON
600 SECOND ST NE
HOPKINS MN 55343

1 MCDONNELL DOUGLAS MISSILE
SYSTEMS CO
ATTN F MCCOTTER
MAILCODE 306 4249
PO BOX 516
ST LOUIS MO 63166-0516

2 INSTITUTE OF ADVANCED TECHLGY
ATTN DR T KIEHNE
DR W G REINEKE
4030 2 W BAKER LANE
AUSTIN TX 78759

1 UNIVERSITY OF CALIFORNIA DAVIS
DEPARTMENT OF MECHANICAL
ENGINEERING
ATTN PROF H A DWYER
DAVIS CA 95616

1 UNIVERSITY OF MARYLAND
DEPARTMENT OF AEROSPACE
ENGINEERING
ATTN DR J D ANDERSON JR
COLLEGE PARK MD 20742

1 UNIVERSITY OF TEXAS
DEPARTMENT OF AEROSPACE
ENGINEERING AND ENGINEERING
MECHANICS
ATTN DR D S DOLLING
AUSTIN TX 78712-1055

1 UNIVERSITY OF FLORIDA
DEPT OF ENGINEERING SCIENCES
COLLEGE OF ENGINEERING
ATTN PROF C C HSU
GAINESVILLE FL 32611

NO. OF
COPIES ORGANIZATION

1 PENNSYLVANIA STATE UNIV
DEPT OF MECHL ENGRG
ATTN DR KENNETH KUO
UNIVERSITY PARK PA 16802

1 FLORIDA ATLANTIC UNIV
DEPT OF MECHL ENGRG
ATTN DR W L CHOW
BOCA RATON FL 33431

1 NORTH CAROLINA STATE UNIV
DEPT OF MECHL & AEROSPACE ENGRG
ATTN PROF D S MCRAE
BOX 7910
RALEIGH NC 27695-7910

1 GEORGIA INSTITUTE OF TECHLGY
SCHOOL OF AEROSPACE ENGRG
ATTN DR WARREN C STRAHLE
ATLANTA GA 30332

2 UNIVERSITY OF ILLINOIS AT
URBANA CHAMPAIGN
DEPT OF MECHL & IND ENGRG
ATTN PROF A L ADDY
PROF CRAIG DUTTON
114 MECHL ENGRG BLDG
1206 WEST GREEN ST
URBANA IL 61801

1 SCIENTIFIC RESEARCH ASSOC
ATTN DR RICHARD BUGGELN
50 NYE RD
PO BOX 1058
GLASTONBURY CT 06033

1 AEDC
CALSPAN FIELD SERVICE
ATTN DR JOHN BENEK
MS 600
TULLAHOMA TN 37389

1 VISUAL COMPUTING
ATTN JEFFREY Q CORDOVA
883 N SHORELINE BLVD
SUITE B210
MOUNTAIN VIEW CA 94043

NO. OF
COPIES ORGANIZATION

1 MDA ENGINEERING INC
 ATTN JOHN P STEINBRENNER
 500 E BORDER ST
 SUITE 401
 ARLINGTON TX 76010

1 CLIMATE CONTROL DIVISION
 PRODUCT ENGINEERING OFFICE
 ATTN TOM GIELDA
 15031 SOUTH COMMERCE DR
 DEARBORN MI 48120

1 CARRIER CORPORATION
 ATTN HOWARD GIBELING
 PO BOX 4808
 CARRIER PARKWAY
 SYRACUSE NY 13221

1 NASA MARSHALL SPACE FLIGHT
 CONTROL CTR
 ATTN KEVIN TUCKER
 MAIL STOP ED 32
 HUNTSVILLE AL 35812

NO. OF
COPIES ORGANIZATION

ABERDEEN PROVING GROUND

31 DIR, USARL
 ATTN: AMSRL-SC,
 MR. W. H. MERGMAGEN, SR.
 DR. W. B. STUREK
 AMSRL-SC-CC,
 MR. C. NIETUBICZ (5 CPS)
 DR. N. PATEL
 AMSRL-WT-P,
 MR. ALBERT HORST
 AMSRL-WT-PB,
 DR. E. SCHMIDT
 DR. M. BUNDY
 DR. K. FANSLER
 MR. E. FERRY
 MR. B. GUIDOS
 MRS. K. HEAVEY
 MR. H. EDGE
 MR. V. OSKAY
 DR. P. PLOSTINS
 DR. A. MIKHAIL
 DR. J. SAHU
 MR. P. WEINACHT
 AMSRL-WT, DR. A. BARROWS
 AMSRL-WT-PD, DR. B. BURNS
 AMSRL-WT-PA,
 DR. T. MINOR
 MR. M. NUSCA
 AMSRL-WT-W, DR. C. MURPHY
 AMSRL-WT-WB, DR. W. D'AMICO
 AMSRL-WT-NC,
 MS. D. HISLEY
 MR. R. LOTTERO
 AMSRL-SL-C, M. MILLER

USER EVALUATION SHEET/CHANGE OF ADDRESS

This Laboratory undertakes a continuing effort to improve the quality of the reports it publishes. Your comments/answers to the items/questions below will aid us in our efforts.

1. ARL Report Number ARL-TR-875 Date of Report October 1995
2. Date Report Received _____
3. Does this report satisfy a need? (Comment on purpose, related project, or other area of interest for which the report will be used.) _____

4. Specifically, how is the report being used? (Information source, design data, procedure, source of ideas, etc.) _____

5. Has the information in this report led to any quantitative savings as far as man-hours or dollars saved, operating costs avoided, or efficiencies achieved, etc? If so, please elaborate. _____

6. General Comments. What do you think should be changed to improve future reports? (Indicate changes to organization, technical content, format, etc.) _____

CURRENT
ADDRESS

Organization

Name

Street or P.O. Box No.

City, State, Zip Code

7. If indicating a Change of Address or Address Correction, please provide the Current or Correct address above and the Old or Incorrect address below.

OLD
ADDRESS

Organization

Name

Street or P.O. Box No.

City, State, Zip Code

(Remove this sheet, fold as indicated, tape closed, and mail.)
(DO NOT STAPLE)

DEPARTMENT OF THE ARMY

OFFICIAL BUSINESS

BUSINESS REPLY MAIL

FIRST CLASS PERMIT NO 0001, APG, MD

POSTAGE WILL BE PAID BY ADDRESSEE

DIRECTOR
U.S. ARMY RESEARCH LABORATORY
ATTN: AMSRL-WT-PB
ABERDEEN PROVING GROUND, MD 21005-5066

NO POSTAGE
NECESSARY
IF MAILED
IN THE
UNITED STATES

